

Nucleus-nucleus reaction cross-sections calculated for realistic nuclear matter distributions within the Glauber-Sitenko approach

V. Lukyanov¹, E. Zemlyanaya¹, B. Slowinski^{2,3},

¹*Joint Institute for Nuclear Research, Dubna, Russia*

²*Faculty of Physics, Warsaw University of Technology, Warsaw, Poland*

³*Institute of Atomic Energy, Otwock-Swierk, Poland*

Abstract. Basing on the thickness (profile) function, previously obtained for the realistic Fermi type distribution of nucleons in nuclei, calculations are made of the microscopic eikonal phases of the nucleus-nucleus scattering and the total reaction cross-sections. In so doing, the phase is deduced to the one-dimensional integral provided that the Gaussian density distribution for the projectile nucleus and an arbitrary shape of the thickness density for the target nucleus are used. The problems of obtaining parameters of the "point" nucleon density are considered. A possibility of approximating the realistic densities by the "surface-matched" Gaussian functions and the dependence of cross-sections on the nucleon-nucleon interaction radius are discussed. The in-medium effects and the role of the trajectory distortion are studied. Conclusions are made on physics of the process, and comparison with experimental data is made with cross sections calculated by using the developed method where no free parameters are introduced.

1 Introduction

In nuclear physics, the Glauber-Sitenko approach [1,2] is used with regard to several its modifications for investigation of nucleus-nucleus collisions at energies of the order of 10÷100 MeV per nucleon of an incident nucleus. In this case, one can determine the eikonal phase by both introducing a model optical potential and using the microscopic approach where it is expressed through density distributions of nuclei and the nucleon-nucleon scattering amplitude.

The parameters of the phenomenological potential $U_{opt}(r) = V(r) + iW(r)$ are usually fitted by comparison of calculations with the experimental differential elastic scattering and total reaction cross-sections. Nevertheless, the problem of ambiguities of obtained parameters still remains [3]. For example, it was shown in [4] that the total reaction cross-section obtained analytically for the Woods-Saxon potential depends, in principle, on two combinations RW_0 and R/a of three parameters, the radius R , diffuseness a and the power W_0 . This fact enables one to specify these latter quantities in the wide limits of their available values. As to the microscopic approach, it does not include, in principle, free parameters, and enables one to calculate the eikonal phases themselves rather than potentials of scattering. It allows one to make predictions of the total reaction cross-sections, including, e.g., those with participation of radioactive nuclei, the important problem related to transmutation of radioactive waste [5, 6].

Beginning with the earlier work [7], the microscopic approach was applied for calculations of proton-nucleus cross-sections. Later on, based on the respective theory of the multiple scattering of nucleons by nuclei [1, 2], it was generalized in [8, 9] to the processes of nucleus-nucleus scattering. This approach was often employed for analysis of interactions of light nuclei with nuclear targets which led, in particular, to the discovery of the neutron halo in 6He , 9Li , the proton halo in ${}^{11}Be$, and the establishment of nuclei with excess of neutrons or protons (see, for instance, [10], and the review papers [11, 12]). Much attention was also given to studying the mechanism of scattering of nuclei and, in particular, to effects of deflection on the

straight-line trajectory of motion [13, 14]. The role of higher order corrections to the eikonal phases [15] and effects of nuclear clusterization [16] were examined, too.

In the majority of such works the use of Gaussian functions (G-functions) for nuclear densities is typical because they make it possible to separate variables in the multidimensional integrals for eikonal phases and, therefore, to obtain results in the analytic form. This is the main reason why G-functions and their modifications are used in calculations of cross-sections even for heavy ions although in this case, of course, the physical reasons require taking the functions of extended shape. In nuclear physics, the Fermi function (F-function) $u_F(r) = [1 + \exp(r - R/a)]^{-1}$ is usually used as the most realistic function for description of densities and potentials of medium and heavy nuclei. Unfortunately, in this case the analytic calculations encounter difficulties. For example, it is impossible to separate variables in the same multidimensional integrals for phases. Nevertheless, F-functions are applied not only in numerical, but also in analytical calculations. In the case of heavy ions these functions are especially needed since they are most realistic ones for description of the shape of potentials and densities in the periphery of collisions of nuclei, the region that forms the elastic differential and total reaction cross-sections. With reference to microscopic approaches the problem is posed to develop analytical methods for calculating cross-sections when using the realistic densities for nuclei with their individual parameters being known from other experiments. In so doing, one can predict with confidence the cross-sections for different combinations of colliding nuclei, and thus to study the genuine mechanism of their interaction. Just such is the goal of the present work.

In Chapter 2 presented is a series of modifications of the origin (initial) microscopic formula for a scattering phase. This is important for both understanding the mechanism of nucleus-nucleus scattering and calculations free of assumptions carried out in many works. In Chapter 3, the explicit expressions for the so-called profile functions of nuclear densities are given in the form of the Gaussian, uniform, and symmetrized (SF) Fermi functions. It is shown how one can reduce the 4-dimensional convolution integral to the one-dimensional one if the density of incident (light) nuclei is presented in the form of G-function and the density of a target nucleus in the form of SF-function. For arbitrary forms of densities the phase is obtained as a one-dimensional integral with the Fourier-Bessel transforms of profiles of densities. The explicit form of such a transform is given for the profile of the SF-density. An inference about the applicability of the so-called modified Gaussian densities is drawn. Chapter 4, is devoted to the problems of using nuclear densities obtained from nuclear form-factors in electron-nuclear scattering, the effects on cross-sections of a choice of the NN-force radius, the distortion of the trajectory of scattering, and the in-medium effects. In Chapter 5, we give the comparison with experimental data and general conclusions.

2 Basic formulae

In the framework of the eikonal approximation and the microscopic approach one can obtain the total reaction cross-sections as follows [1, 2]:

$$\sigma_R = 2\pi \int_0^\infty db b \left(1 - e^{-\chi(b)}\right), \quad (2.1)$$

where the phase

$$\chi(b) = \bar{\sigma}_{NN} \mathcal{I}(b) \quad (2.2)$$

is determined by the isospin average total nucleon-nucleon cross-section

$$\bar{\sigma}_{NN} = \frac{Z_p Z_t \sigma_{pp} + N_p N_t \sigma_{nn} + (Z_p N_t + N_p Z_t) \sigma_{np}}{A_p A_t} \quad (2.3)$$

and the folding integral that, in the case of the nucleus-nucleus scattering, has the form [8, 9]

$$\mathcal{I}(b) = \int d^2 s_p d^2 s_t \rho_p^\circ(s_p) \rho_t^\circ(s_t) f(\xi), \quad \xi = \mathbf{b} - \mathbf{s}_p + \mathbf{s}_t. \quad (2.4)$$

Here vectors \mathbf{s} , ξ are displayed in the impact parameter b plane perpendicular to the oz axis along the momentum \mathbf{k}_i of the incident nucleus ¹, and $\rho^\circ(s)$ are the so-called thickness (profile) functions of density distributions of centers of nucleons ("point-like nucleons") of the incident nucleus (with the atomic number A_p) and the target nucleus A_t ². The thickness densities are given as

$$\rho(s) = \int_{-\infty}^{\infty} dz \rho(\sqrt{s^2 + z^2}). \quad (2.5)$$

The point nucleon profiles $\rho^\circ(r)$ differ from the matter distributions $\rho(r)$ in nuclei composed of real, i.e. "dressed" nucleons. So, when using the convolution integral (2.4) we need be concerned with obtaining the point-like densities $\rho^\circ(r)$ from the "experimental" nuclear densities $\rho(r)$. Just for $\rho(r)$ a large set of tabulated data exists obtained from electron-nucleus scattering data ³, and our goal is to develop the approach in such a way that to use in calculations the table data for $\rho(r)$ and do not introduce free parameters.

The function $f(\xi)$ determines the form of the nucleon-nucleon interaction amplitude

$$f(\xi) = (\sqrt{\pi} a_N)^{-2} e^{-\xi^2/a_N^2}, \quad a_N^2 = \frac{2}{3} r_{N \text{ rms}}^2. \quad (2.6)$$

Here $r_{N \text{ rms}}^2$ is the root-mean-square radius of NN-interaction, and $a_N^2 = 2\beta$ is expressed by the shape parameter β of the scattering amplitude of nucleons⁴ in the form $\exp(-q^2\beta/2)$. The values of β at energy of the order of 1 GeV are in the interval $0.21 \div 0.23 \text{ fm}^{-2}$ [18] which means that $r_{N \text{ rms}}^2 = 0.63 \div 0.69 \text{ fm}^2$. In our case the nucleon-nucleon forces act in nuclear medium, and

¹ In [17] a similar expression was obtained in the model of interacting tubes of the nucleon fluxes in collided nuclei.

² Here \mathbf{s} and \mathbf{r} are vectors in the 2- and 3-dimensional spaces, and $r^2 = s^2 + z^2$. Then, $\rho(r)$ and $\rho^\circ(r)$ are the density distributions, and $\rho(s)$ and $\rho^\circ(s)$ are their profiles, respectively.

³ In general, one-particle densities $\rho(r)$ depend on coordinates in the respective center-of-mass frame of a nucleus. However, as usual, in analysis of form factors of nuclei, one omits the respective factor of the center-of-mass motion $\exp(q^2\langle q^2 \rangle/6A)$, where $\langle r^2 \rangle$ and A are the root-mean-square radius and a mass number of the nucleus. Therefore, the tabulated $\rho(r)$ appear to be distributions of a nuclear charge (or matter) in the field of a fixed nuclear potential. At small q and large A densities in both systems coincide.

⁴ The amplitude is $f_N(q) = f_N(0) f(q)$, where $f_N(0) = (k_N/4\pi) \bar{\sigma}_{NN}(i + \alpha_{NN})$, and k_N is the relative momentum of colliding nucleons. For $f(q) = \exp(-q^2 a_N^2/4)$ the Bessel-Fourier transform $f(\xi) = (2\pi)^{-2} \int \exp(-i\mathbf{q}\xi) f(q) d^2 q$ follows eq.(2.6), and in the zero-range approximation ($a_N = 0$), when $f(q) = 1$, one gets the delta-function in 2-dimensional space, i.e. $f(\xi) = \delta^{(2)}(\xi)$.

to take into account their influence the correction factor f_m is additionally introduced under the integral. Later on we will touch this problem in detail.

The convolution integral (2.4) has a similar form as the 6-dimensional "double folding" integral in calculation of the nucleus-nucleus potential [19]. In both the cases we are led to search for the ways of separating variables in integrands. In Chapter 3 we show that the integral (2.4) can be calculated explicitly if both densities are the G-functions, or it is reduced to the one-dimensional integral when one of the densities has the Gaussian form. At the same time, there exists a standard procedure to transform such integrals to one-dimensional ones in the momentum space. To this end, in each function in (2.4) one should perform the two-dimensional Fourier-Bessel transformation

$$u(s) = \frac{1}{(2\pi)^2} \int e^{-i\mathbf{ks}} \tilde{u}(k) d^2k = \frac{1}{2\pi} \int_0^\infty J_0(ks) \tilde{u}(k) k dk, \quad (2.7)$$

where

$$\tilde{u}(k) = \int e^{i\mathbf{ks}} u(s) d^2s = 2\pi \int_0^\infty J_0(ks) u(s) s ds. \quad (2.8)$$

Then (2.4) becomes

$$\mathcal{I}(b) = \frac{1}{2\pi} \int_0^\infty k dk J_0(kb) \tilde{\rho}_p(k) \tilde{\rho}_t(k) \tilde{f}(k), \quad (2.9)$$

where

$$\tilde{f}(k) = \exp(-k^2 r_{N \text{ rms}}^2 / 6). \quad (2.10)$$

Next, using the convolution formula for the nuclear thickness density

$$\rho_i(s) = \int d^2s_N \rho_N(s_N) \rho_i^\circ(|\mathbf{s} - \mathbf{s}_N|), \quad (2.11)$$

where $\rho_N(s_N)$ is the nucleon thickness density, one obtains with the help of (2.7) the following result:

$$\tilde{\rho}_i(k) = \tilde{\rho}_N(k) \tilde{\rho}_i^\circ(k). \quad (2.12)$$

For the Gaussian density of a nucleon with the r_{rms} radius one has

$$\tilde{\rho}_N(k) = \exp\left(-\frac{k^2 r_{0 \text{ rms}}^2}{6}\right). \quad (2.13)$$

Then, (2.9) results in

$$\mathcal{I}(b) = \frac{1}{2\pi} \int_0^\infty k dk J_0(kb) \tilde{\rho}_p^\circ(k) \tilde{\rho}_t(k) \exp\left(-\frac{k^2 \tau^2}{6}\right), \quad (2.14)$$

$$\tau^2 = r_{N \text{ rms}}^2 - r_{0 \text{ rms}}^2. \quad (2.15)$$

If it is considered that $r_{N \text{ rms}}^2$ and $r_{0 \text{ rms}}^2$ coincide, then $\tau^2 = 0$ and so

$$\mathcal{I}(b) = \frac{1}{2\pi} \int_0^\infty k dk J_0(kb) \tilde{\rho}_p^\circ(k) \tilde{\rho}_t(k), \quad (2.16)$$

and in the coordinate representation

$$\mathcal{I}(b) = \int_0^\infty d^2s \rho_p^\circ(|\mathbf{b} - \mathbf{s}|) \rho_t(s). \quad (2.17)$$

As a result, we have obtained the expressions for convolution integrals (2.14),(2.16),(2.17), where the thickness functions $\rho_t(s)$ (or $\tilde{\rho}_t(k)$) come into being instead of profiles of the target-nucleus "point-like" densities. Just for them the respective "experimental" densities are usually known from tables where they are parametrized for heavy and middle-weight nuclei in the form of a Fermi function. In principle, one can employ eqs.(2.12) and (2.13) for incident nuclei as well, i.e. one uses $\tilde{\rho}_p^\circ = \tilde{\rho}_p/\tilde{\rho}_N$. But then under the integrals (2.14),(2.16) an increasing Gaussian function appears, and if for the profiles of both the densities the functions with realistic exponential asymptotics are taken, then the integrals will diverge at the upper limit. Of course, one can act formally, i.e. either "cut" integration at the point where an integrand starts to increase, or change the Gauss-like nucleon form-factor (2.13) by a dipole formula (see below eq.(4.2)). On the other hand, if for the density of one of the nuclei one takes a Gauss function, then no divergence arises.

Finally, it should be mentioned that in some papers the so-called zero-range approximation ($r_{N\,rms}^2 = 0$) is used. This leads to the convolution integral in the form (2.9) with $\tilde{f}(k)=1$, or, in the spatial coordinates, in the form (2.17) with $\rho_t^\circ(s)$ in(2.17) instead of $\rho_t(s)$. A rougher approach is when both the densities in (2.17) are supposed to be the nuclear ones $\rho(s)$. Now we see that such approaches are not necessary to be used, and they themselves distort the true mechanism of nucleus-nucleus scattering.

3 Eikonal phases for realistic density distributions

As mentioned above, to obtain analytic expressions for phases and cross-sections the Gaussian (G-functions) density distributions and their profiles are used

$$\rho_G(r) = \rho_G(0) e^{-r^2/a_G^2}, \quad \rho_G(0) = A/(\sqrt{\pi}a_G)^3, \quad (3.1)$$

$$\rho_G(s) = (\sqrt{\pi}a_G) \rho_G(0) e^{-s^2/a_G^2}, \quad a_G^2 = \frac{2}{3}R_{rms}^2, \quad (3.2)$$

where the only parameter a_G is determined by the root-mean-square nuclear radius R_{rms} ⁵.

We also list the functions of uniform density distribution and the relevant profiles

$$\rho_u(r) = \rho_u(0) \Theta(R_u - r), \quad \rho_u(0) = 3A/4\pi R_u^3, \quad (3.3)$$

$$\rho_u(s) = \rho_u(0) \sqrt{R_u^2 - s^2} \Theta(R_u - s), \quad R_u^2 = \frac{5}{3}R_{rms}^2, \quad (3.4)$$

which are sometimes used for middle and heavy nuclei.

In principle, the realistic density having the Fermi distribution (F-function) can be approximated by a sum of Gaussian functions with by fitting expansion coefficients and parameters

⁵ For the point density $\rho_G^\circ(r)$, the parameter $a_G^{\circ 2} = \frac{2}{3}R_{rms}^2$ can be expressed through the respective *rms*-radius $R_{rms}^2 = R_{rms}^2 - r_{0\,rms}^2$.

a_G . Such a procedure was suggested in [20], and in [21] this one was proposed not to densities but directly to profiles of Fermi functions. Unfortunately, this procedure must be repeated at every new set of parameters R and a of the initial F-functions. However, one can remind that for heavy ions, both differential elastic scattering and total reaction cross-sections are first determined by the behavior of phases in a periphery of collisions. It seems likely that the first attempt to model the tail of the F-distribution $\rho_F(r)$ with the help of *one* Gaussian function was made in [22]. Later on in [23], not a Fermi density but its profile $\rho_F(s)$ was reproduced in such a way. For this aim the G- and F-functions were matched in their periphery to find two parameters $a_{\bar{G}}$ $\rho_{\bar{G}}^o(0)$ of the so-called modified G-function

$$\rho_{\bar{G}}(s) = (\sqrt{\pi} a_{\bar{G}}) \rho_{\bar{G}}(0) e^{-s^2/a_{\bar{G}}^2}. \quad (3.5)$$

This function is not normalized, since its parameters are no longer connected mutually in such a way as in (3.1). In the general case, when matching $\rho_{\bar{G}}(s)$ with an arbitrary form of the extended function $\rho(s)$ at two points s_1 and s_2 we obtain two parameters of (3.5)

$$\rho_{\bar{G}}(0) = (\sqrt{\pi} a_{\bar{G}})^{-1} \rho(s_1) \exp(s_1^2/a_{\bar{G}}^2), \quad (3.6)$$

$$a_{\bar{G}} = \left[\frac{s_2^2 - s_1^2}{\ln \rho(s_1) - \ln \rho(s_2)} \right]^{1/2}. \quad (3.7)$$

In [23], the points of matching the \bar{G} - and F-profiles have been taken as $s_1 = c$ and $s_2 = c + 4d$ where c and d are the radius and diffuseness parameters, and the profiles $\rho_F^o(s)$ were obtained by numerical integration in (2.5). Herewith d was assumed to be the same $d = 0.53 \text{ fm}$ for all nuclei, and c was determined from the known *rms* radii of nuclei and nucleon R_{rms} and r_{0rms} with the help of the formula

$$R_{rms}^2 = R_{rms}^2 - r_{0rms}^2 = \frac{3}{5}c^2 \left[1 + \frac{7}{3} \left(\frac{\pi d}{c} \right)^2 \right]. \quad (3.8)$$

In general, the accuracy of such a matching should be checked every time since the nuclear Fermi densities $\rho_F(r)$ have different values of a for different nuclei. Besides, the obtained parameters of \bar{G} -functions depend on a choice of matching points.

Starting with [24] the symmetrized SF-function

$$u_{SF}(r) = \frac{\sinh R/a}{\cosh R/a + \cosh r/a} = \frac{1}{1 + \exp \frac{r-R}{a}} - \frac{1}{1 + \exp \frac{r+R}{a}}. \quad (3.9)$$

has come into use, first, in calculations of nuclear form factors in eA-scattering, and next, in other problems of nuclear physics, too. This function has several advantages as compared to the F-function, allowing much room for analytical calculations [25], [26]. Its shape is the universal one for a satisfactory modelling the nuclear densities of light, middle and heavy nuclei [27]. It is evident from (3.9) that for middle and heavy nuclei ($R \gg a$) this function in fact coincides with the usual Fermi function $u_F(r) = 1/(1 + \exp[(r - R)/a])$. Therefore, parameters of this function can be taken from the existing Tables of Fermi distributions for both nuclear densities [28] and point-like densities of nuclei [29]. For our task it is important that just for the SF-function the respective profile was obtained in an explicit form [30] and therefore the following calculations can be considerably simplified. So, the SF-density distribution and its profile have the following form (3.10) (3.11):

$$\rho_{SF}(r) = \rho_{SF}(0) \frac{\sinh R/a}{\cosh R/a + \cosh r/a}, \quad \rho_{SF}(0) = \frac{3A}{4\pi R^3} \left[1 + \left(\frac{\pi a}{R} \right)^2 \right]^{-1}, \quad (3.10)$$

$$\rho_{SF}(s) = 2R \rho_{SF}(0) \frac{\sinh R/a}{\cosh R/a + \cosh s/a} P(s). \quad (3.11)$$

Here the main dependence of the profile on s is determined by SF-function with the same parameters as in the density $\rho_{SF}(r)$. The corrective factor $P(s)$ is presented in [30] and specified with the help of the auxiliary function $x(s)$. This latter obeys the condition $x(s) \ll 1$ which allows one to simplify $P(s)$, so that it arrives at

$$P(s) = \frac{a}{R} \ln(4/x(s)), \quad x(s) = \frac{2}{\kappa} \frac{\cosh s/a}{\cosh s/a + \cosh R/a} \left\{ 1 + \frac{\kappa - 1}{\cosh s/a} \right\}. \quad (3.12)$$

Here κ is expressed by the radius R and diffuseness a as

$$\kappa = e^\delta, \quad \delta = 1.10315 + 0.34597(R/a) - 0.00446(R/a)^2. \quad (3.13)$$

The numerical values of the coefficients in (3.13) were found in [30] by fitting the profile (3.11) to numerical values of the profile integral (2.5) for $\rho_{SF}(r)$ (3.10) in the region of $5 \leq R/a \leq 20$. In the center of a nucleus one has $P(0) = 1$, and in the region of the main contribution from $s = R$ to ∞ it changes a little by $\simeq 0.4(a/R)$. This enables one to take $P(s)$ at one point only, for example, at $s = R$, or at $s = s_{1/3} = R + a \ln 2$, where the density itself falls by three times⁶. Then, if $\cosh R/a \gg \kappa$, one obtains

$$P(R) \simeq \frac{a}{R} [\ln 4\kappa] = \frac{a}{R} \left[2.48945 + 0.34597 \frac{R}{a} - 0.00446 \left(\frac{R}{a} \right)^2 \right], \quad (3.14)$$

and, respectively,

$$\rho_{SF}(s) \simeq 2R \rho_{SF}(0) \frac{\sinh R/a}{\cosh R/a + \cosh s/a} P_a(R). \quad (3.15)$$

In Fig.1 are shown the profiles of SF-density for three nuclei: ^{16}O , ^{40}Ca , ^{208}Pb , calculated numerically (points) using eq.(2.5), and the corresponding \bar{G} -profiles (dashes), matched according to (3.6), (3.7) at R and $R + 4a$. Full curves represent $\rho_{SF}(s)$ calculated with the help of the analytic formula (3.11). The parameters of SF-densities are taken from [27] and are given in Table 1. One can see that a strong discrepancy exists between \bar{G} -profiles and the initial SF-profiles in the inner region (for example, by two orders of magnitude for ^{208}Pb), and also in the region where the density falls off by two orders of magnitude and more. The profiles of the uniform and Gaussian forms differ much more from the profiles of the Fermi function. In Fig.2, the functions $\rho_{SF}(s)$ are depicted for the same nuclei but calculated within analytic formulae: full - by (3.11) with the exact corrective factor $P(s)$, and dashed lines - by eq. (3.15) with the approximated one $P_a(s = R)$. It turns out that the use of the corrective factor at the radius point practically does not change the behavior of profile functions in the

⁶ It was established in [19] that the behavior of the nucleus-nucleus scattering is responsible for the region where densities overlap in their periphery at $s \geq s_{1/3}$.

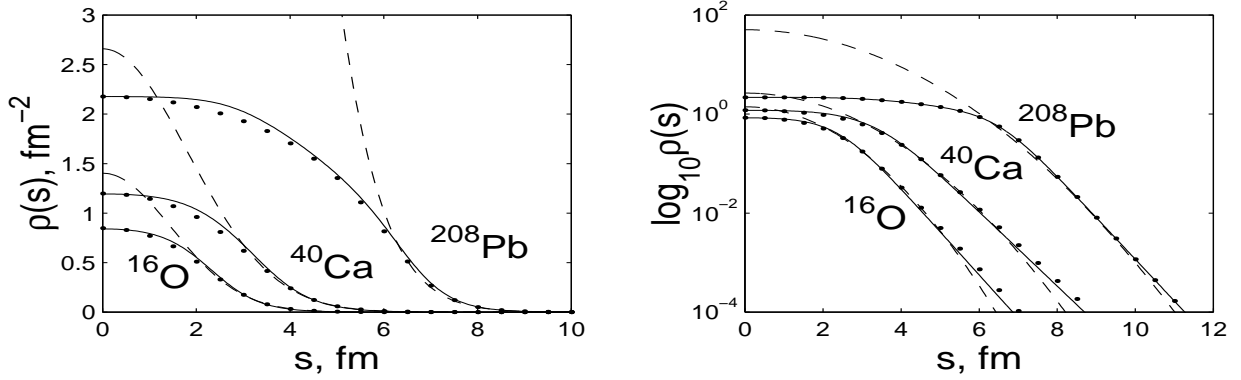


Figure 1: Thickness functions for SF-densities. Bold dots – numerical integration of eq.(2.5), dashes – \bar{G} -profiles adjusted to the bold dots curves. Solid curves – SF-thickness densities calculated by analytic eq.(3.11). Parameters are in Table 1.

peripheral region. A slight difference, no more than a factor of two for ^{208}Pb , appears in the inner region only, which is far less than it is observed in Fig.1 when one uses the $\bar{G}(s)$ -functions.

Table 1. *Parameters of nuclear symmetrized Fermi density distributions $\rho_{SF}(r, R, a)$ ⁷.*

Nucleus	R, fm	a, fm	R_{rms}, fm	Ref.
^{12}C	2.214	0.488	2.496	[27]
^{16}O	2.562	0.497	2.711	[27]
^{20}Ne	2.74	0.572	3.004	[28]
^{24}Mg	2.934	0.569	3.105	[27]
^{27}Al	3.07	0.519	3.06	[28]
^{28}Si	3.085	0.563	3.175	[27]
^{32}S	3.255	0.601	3.370	[27]
^{40}Ca	3.556	0.578	3.493	[27]
^{66}Zn	4.340	0.559	3.952	[28]
^{89}Y	4.86	0.542	4.27	[28]
^{208}Pb	6.557	0.515	5.427	[27]

So, in the subsequent discussion we have a possibility of choosing the profiles $\rho(s)$ of the explicit analytic form for different nuclear densities, namely, for the Gaussian, uniform and symmetrized Fermi functions. Below they will be used in calculations of microscopic eikonal phases $\chi(b)$ and total reaction cross-sections.

First we consider the convolution integral (2.17) where the thickness density of an incident nucleus $\rho_p^\circ(\zeta)$ is taken in the Gaussian form (3.5). If one substitutes into (2.17) the expression

$$\rho_{\bar{G},p}^\circ(|\vec{b} - \vec{s}|) = (\sqrt{\pi}a_{\bar{G},p}^\circ) \rho_{\bar{G},p}^\circ(0) \exp\left[-\frac{1}{a_{\bar{G},p}^\circ 2} (b^2 - 2bs \cos \varphi + s^2)\right] \quad (3.16)$$

⁷ Parameters of the Fermi-distributions $\rho_F(r, R, a)$, taken from [28], are very close to those of $\rho_{SF}(r, R, a)$ for the given three nuclei

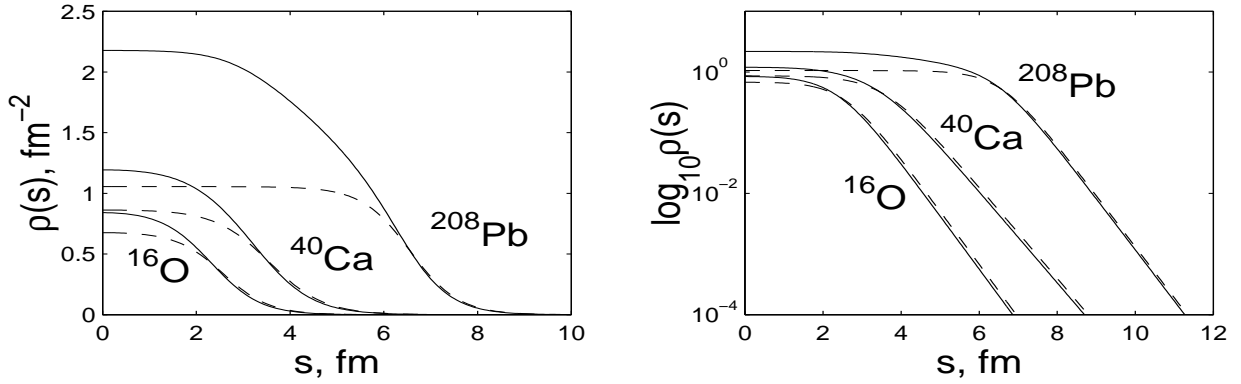


Figure 2: Comparison of the SF-thickness densities calculated by analytic eq.(3.11) with the exact correction function $P(s)$ (solid curves), with the approximate $P(s=R)$ by eq.(3.15). Parameters are the same as in Fig.1.

and integrates over φ by using the definition of the Bessel function $I_0(x)$ [31] of an imaginary argument, it follows:

$$\mathcal{I}_{\bar{G},t}(b) = 2\pi(\sqrt{\pi}a_{\bar{G},p}^\circ)\rho_{\bar{G},p}^\circ(0)\exp\left(-\frac{b^2}{a_{\bar{G},p}^{\circ 2}}\right)\int_0^\infty sds \rho_t(s) \exp\left(-\frac{s^2}{a_{\bar{G},p}^{\circ 2}}\right) I_0\left(\frac{2bs}{a_{\bar{G},p}^{\circ 2}}\right). \quad (3.17)$$

In a more general case, when the magnitudes of *rms* radii of the nucleon and NN-interaction differ, it is convenient to use the convolution integral (2.4) with profiles of point-like densities for both nuclei. Then one can show that in the case of the \bar{G} -thickness density of an incident nucleus (3.5) the convolution integral takes the form:

$$\begin{aligned} \mathcal{I}_{\bar{G},N,t}(b) = 2\pi \frac{a_{\bar{G},p}^{\circ 2}}{a_{\bar{G},p}^{\circ 2} + a_N^2} (\sqrt{\pi}a_{\bar{G},p}^\circ)\rho_{\bar{G},p}^\circ(0) \exp\left(-\frac{b^2}{a_{\bar{G},p}^{\circ 2} + a_N^2}\right) \times \\ \times \int_0^\infty sds \rho_t^\circ(s) \exp\left(-\frac{s^2}{a_{\bar{G},p}^{\circ 2} + a_N^2}\right) I_0\left(\frac{2bs}{a_{\bar{G},p}^{\circ 2} + a_N^2}\right). \end{aligned} \quad (3.18)$$

If for a target-nucleus one also takes the Gaussian function, then integration in (3.19) is performed explicitly [31], and one obtains [22]

$$\mathcal{I}_{\bar{G},N,\bar{G}}(b) = \frac{1}{\pi} \frac{(\sqrt{\pi}a_{\bar{G},p}^\circ)^3(\sqrt{\pi}a_{\bar{G},t}^\circ)^3}{a_{\bar{G},p}^{\circ 2} + a_{\bar{G},t}^{\circ 2} + a_N^2} \rho_{\bar{G},p}^\circ(0)\rho_{\bar{G},t}^\circ(0) \exp\left(-\frac{b^2}{a_{\bar{G},p}^{\circ 2} + a_{\bar{G},t}^{\circ 2} + a_N^2}\right). \quad (3.19)$$

Note that in the case of normalized Gaussian functions (3.1) it is necessary to change \bar{G} by G in (3.17) - (3.19), and put $(\sqrt{\pi}a_i^\circ)^3\rho_{G,i}^\circ(0) = A_i$.

We imply that the realistic density distributions of middle and heavy nuclei are the (symmetrized) Fermi functions. Their profile functions (3.10) and (3.15) are known in a certain form. The Bessel functions $I_0(x)$ and $J_0(x)$ are also known explicitly in the form approximated by polynomials [32]. So all functions in the convolution integrals (3.17) and (3.18) are given explicitly which is highly feasible for numerical integration.

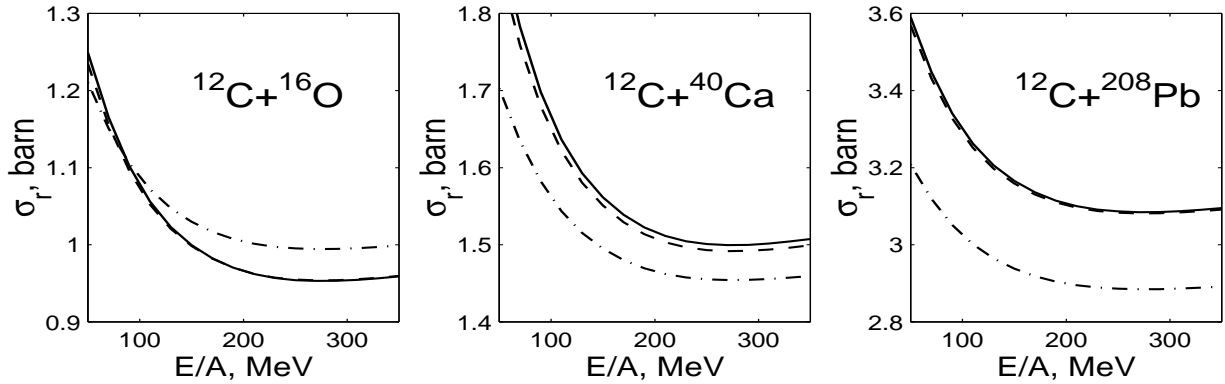


Figure 3: Total reaction cross-sections for different thickness densities. The \bar{G} -profile of the projectile nucleus ^{12}C is adjusted to its SF-point-like thickness density having parameters from Table 2. For the target-nuclei, solid curves are for the SF-densities (parameters in Table 1), dashes-dots – for unified densities, dashes – \bar{G} -model.

In the case when the density distributions of both the nuclei are given as the SF-functions, it is reasonable to use the convolution integrals in the momentum representation (2.9), (2.14) or (2.16). Then, it is convenient to take their thickness functions approximated by (3.15); as a result, the Fourier transform can be easily calculated. Indeed, inserting (3.15) into (2.8) one obtains

$$\tilde{\rho}_{SF}(k) = 4\pi R \rho_{SF}(0) P_a(R) \mathcal{F}_{SF}(k, a, R), \quad (3.20)$$

where

$$\mathcal{F}_{SF}(k, a, R) \equiv \mathcal{F}_{SF}(k) = \int_0^\infty s ds J_0(ks) \frac{\sinh R/a}{\cosh R/a + \cosh s/a}. \quad (3.21)$$

Taking into account the peripheral nature of nucleus-nucleus collisions one can assume that the main contribution is made in the region when $ks \gg 1$. Then (see, e.g., [33]) we have

$$\mathcal{F}_{SF}(k) = \frac{\pi a R}{\sinh \pi a k} J_1(kR). \quad (3.22)$$

In [25], the higher order corrections to (3.22) are established but they do not give significant contributions at $kR \gg 1$.

In Fig.3 are shown the calculated total reaction cross-sections for collisions of ^{12}C with ^{16}O , ^{40}Ca , ^{208}Pb at energies from 50 to 350 MeV/nucleon. For the target-nuclei, different nuclear densities are chosen in the form of SF-functions, modified \bar{G} -functions and U-functions of uniform distribution. The convolution integral (3.17) has been used for the χ -phase. The profile function \bar{G} for the incident nucleus ^{12}C was shifted at $s_1 = c$ $s_2 = c + 4a$ (see (3.5)-(3.7)) with the profile of the corresponding point-like SF-density whose parameters are given in Table 2. When one tested \bar{G} -profiles for the target-nuclei, the parameters of their densities ρ_{SF} were taken from Table 1. The R_{rms} -radii which have been used in calculations of the uniform distribution radius R_u (3.4) are also quoted in Table 1. The energy-depended total nucleon-nucleon cross-sections σ_{NN} are taken from [23]. One can see that for a uniform density, the total reaction cross-sections (dot-and-dash curves) have highly different forms as compared to ones for the physically justified SF-densities (full lines). Besides, both calculations with the SF and \bar{G} -models (dashed) are close to each other. A slight excess of cross-sections for SF-functions

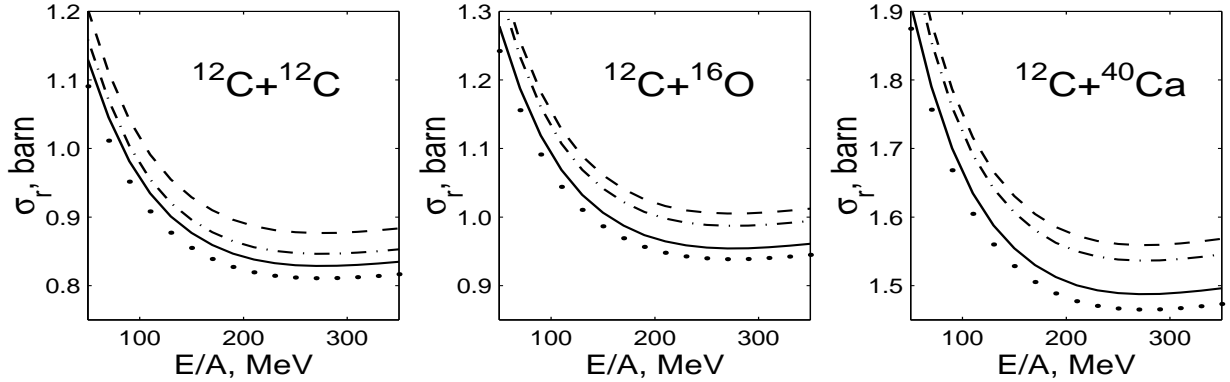


Figure 4: Dependence of cross-sections on the point-like density parameters obtained from eA -scattering data. Solid curves – with parameters from Table 2, dashed curves – with parameters given by eq.(4.4); dashes-dots – parameters from [37]; bold circles – calculations in the momentum representation using eq.(3.20) (see the text).

at low energies results from their extended "tails". Instead, a weak relative increase in cross-sections at higher energies for the \bar{G} -functions of the target-nuclei is due to their larger values in the inner nuclear region, which leads to the earlier "activation" of absorption as compared to the SF-model.

The cross-section calculations in the momentum representation with utilizing the realistic ρ_{SF} -densities and the approximate correction $P_a(R)$ -function (3.14), and the related approximate profiles (3.15) and (3.20) show (see Fig.4) a slight difference $\approx 2\%$ of such calculations ("bold" points) from the exact ones (solid curves).

Table 2. Parameters of the symmetrized Fermi density distributions $\rho_{SF}^\circ(r, c, d)$ of the point-like nucleons in nuclei [29].

Nucleus	^{12}C	^{16}O	^{24}Mg	^{28}Si	^{32}S	^{40}Ca
$c, \text{ fm}$	2.275	2.624	2.984	3.134	3.291	3.593
$d, \text{ fm}$	0.393	0.404	0.484	0.477	0.520	0.493

4 Calculations and discussion

4.1 On the use of nuclear densities from eA -scattering

The convolution integrals (2.4) and (2.9) depend on profiles of both nuclei composed of point-like densities $\rho^\circ(s)$, while the transformed integrals (2.16), (2.17) include only one density $\rho^\circ(s)$ whereas the other density is the nuclear one $\rho(s)$. So the problem of obtaining point-like densities of nuclei is not elucidated completely, and we consider how they can be extracted from existing data. In general, one can calculate them in the framework of nuclear models. However, from the outset we posed the task of using primarily the data of other experiments,

for instance, the data on nuclear charge form factors. In this case we consider, so far, that the realistic point-like densities have the form $\rho_{(S)F}^\circ(r)$.

The first method [29] is based on the representation of a nuclear ("experimental") form factor in the form like (2.12) as follows:

$$F(q) = F_P(q) F^\circ(q). \quad (4.1)$$

Here $F^\circ(q)$ is the form factor of a nucleus with point-like nucleons and $F_P(q)$ is the proton form factor presented by the dipole formulae which can be approximated at small momentum by the Gaussian function

$$F_P(q) = \left(1 + \frac{q^2 r_{0rms}^2}{12}\right)^{-2} \simeq \exp(-q^2 r_{0rms}^2/6). \quad (4.2)$$

Then, the obtained $F^\circ(q)$ is analyzed within the model-independent method to obtain a point-like density $\rho^\circ(r)$ as a sum of the $\rho_{SF}^\circ(r)$ -function with its derivatives multiplied by the fitted coefficients. The latter reproduce the so-called radial variations of densities. In this procedure, every $F^\circ(q)$ with the respective trial density $\rho^\circ(r)$ is calculated in the high-energy approximation [34], [35], the analytical method which gives results in close agreement with numerical solutions of the Dirac equation. In Table 2 we reproduce part of data from [29], namely, the radii c and diffuseness d parameters of densities $\rho_{SF}^\circ(r, c, d)$ excluding the radial variations which play an important role only at large q . In [29], the employed proton $r_{0rms}^2 = 0.658 \text{ fm}^2$ slightly differs from $r_{0rms}^2 = 0.65 \text{ fm}^2$, the matter r_{0rms}^2 , which was used in calculations of the double-folding potentials [19]. However, by this reason the point-like densities from [29] can be related to the nucleon distributions $\rho_{SF}^\circ(r)$ rather than to the proton ones⁸.

The other method [36] of obtaining c and d parameters of $\rho^\circ(r, c, d)$ is based on approximate analytic calculations of r^n -moments of densities $\rho_F(r, R, a)$, where the latter is given by its folding form like (2.11). The obtained explicit results for moments are compared with those obtained by using the standard form $\rho_F(r, R, a)$ and lead to

$$c = R \left[1 + \frac{1}{3} \left(\frac{r_{0rms}}{R} \right)^2 \right], \quad d = a \left[1 - \frac{1}{2} \left(\frac{r_{0rms}}{\pi a} \right)^2 \right]. \quad (4.3)$$

In evaluations, terms of orders higher than $(\pi a/R)^2$ and $r_{0rms}^2/9c^2$ were neglected. If one inserts parameters R and a of $\rho_{SF}(r, R, a)$ from Table 1 and $r_{0rms}^2 = 0.658 \text{ fm}^2$ into equations (4.3), and compares the obtained values with the respective parameters from Table 2, one discloses the former to be smaller as compared to those in Table 2 (about 1% for c and not more than 10% for d). The effect of this discrepancy on the corresponding total reaction cross sections is shown in Fig.4. The solid curves are calculations with parameters c and d from Table 2. The dashed curves are with using c and d , estimated by eq.(4.3) at R and a from Table 1. The dash-dotted curves show the cross-sections for c and d from [37] (^{12}C : 2.1545, 0.425; ^{16}O : 2.525, 0.45; ^{40}Ca : 3.60, 0.523), where they were used in calculations of the real parts of nucleus-nucleus folding potentials to explain the elastic scattering cross-sections at energies of about 10 MeV/nucleon. In all the cases we take $r_{Nrms}^2 = 0.658 \text{ fm}^2$. One can see that for every set of colliding nuclei differences between the respective cross-sections occur in

⁸ If one assumes the relation between proton and neutron densities to be $\rho_N^\circ(r) = (N/Z)\rho_Z^\circ(r)$ and takes r_{rms} of densities of nuclei consisting of nucleons R_{rms}^2 , the point-like nucleons \mathcal{R}_{rms}^2 , and protons $\langle r^2 \rangle_P = 0.76 \text{ fm}^2$ and neutrons $\langle r^2 \rangle_N = -0.11 \text{ fm}^2$ (see [19]), then it follows from $R_{rms}^2 = \mathcal{R}_{rms}^2 + \langle r^2 \rangle_P + \langle r^2 \rangle_N = \mathcal{R}_{rms}^2 + \langle r^2 \rangle$ that the r_{rms} -radius of a nucleon is $\langle r^2 \rangle = \langle r^2 \rangle_P + \langle r^2 \rangle_N = 0.65 \text{ fm}^2$.

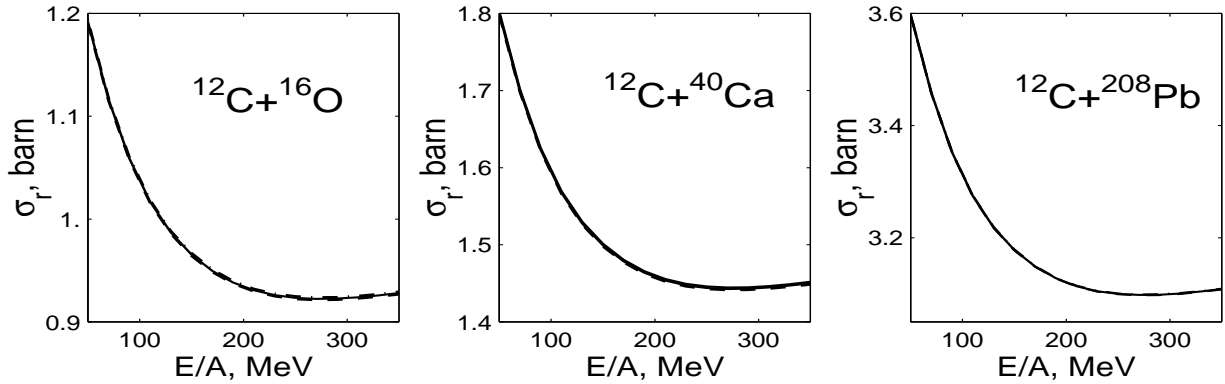


Figure 5: Dependence of cross-sections on the NN-interaction radius: $r_{N\,rms}^2 = 0.658 \text{ fm}^2$ (solid curves), 0.630 fm^2 (dots), 0.69 fm^2 (dash-dots). Parameters c and d for ^{16}O and ^{40}Ca are in Table 2, and for ^{208}Pb they are done by eq.(4.4) with R and a from Table 1. For ^{12}C the \bar{G} -profile is the same as in Fig.3.

the limits of $\approx 6 \div 10\%$. Nevertheless, we incline to believe that a more rigorous method of obtaining point-like density parameters is to analyze the $F^\circ(q)$ form factors of nuclei, and thus it is important to make up Tables of the respective densities.

4.2 On establishing NN-interaction radius

It was shown in Sec.2 that at the same radii of the nucleon and NN-interaction $r_{0\,rms}^2 = r_{N\,rms}^2$ the convolution integral is reduced to a simpler form (2.17) which contains only thickness functions of nuclear matter distribution of a target-nucleus and the point-like density of a projectile nucleus. As to the NN-interaction parameter $a_N^2 = (2/3)r_{N\,rms}^2$, it is known from the scattering data of free nucleons to give $r_{N\,rms}^2$ in the limits of $0.63 \div 0.69 \text{ fm}^2$. At the same time, in the dipole formula, the nucleon *rms*-radius $r_{0\,rms}^2$ was used as 0.658 fm^2 [29], and in calculations of the double-folding potential [19] it was taken to be 0.650 fm^2 . The effect of their differences on the reaction cross-sections is seen from Fig.5. In calculations, convolution integrals were taken in the form (3.18). The parameters c d of the point densities for ^{12}C , ^{16}O , ^{40}Ca are given in Table 2, and for ^{208}Pb they were evaluated using eq.(4.3). For the projectile nucleus ^{12}C we used \bar{G} -profile adjusted to the respective thickness SF-density in the same manner as for Fig.3. It is seen from Fig.5 that the obtained cross-sections, in fact, coincide to each others. Therefore, the study of total cross-sections does not allow us to distinguish between *rms* radii of a nucleon and the NN-interaction. Moreover, one should bear in mind that the amplitude of scattering of free nucleons and its parameter a_N can differ from those scattered in nuclear medium.

4.3 Influence of the trajectory distortion

In the repulsive Coulomb field the trajectory of an incident nucleus deflects from the scattering center, which results in decrease of the total reaction cross-section. This effect was taken into account in [38] by replacing, in the phase $\chi(b)$, the impact parameter b by the distance of

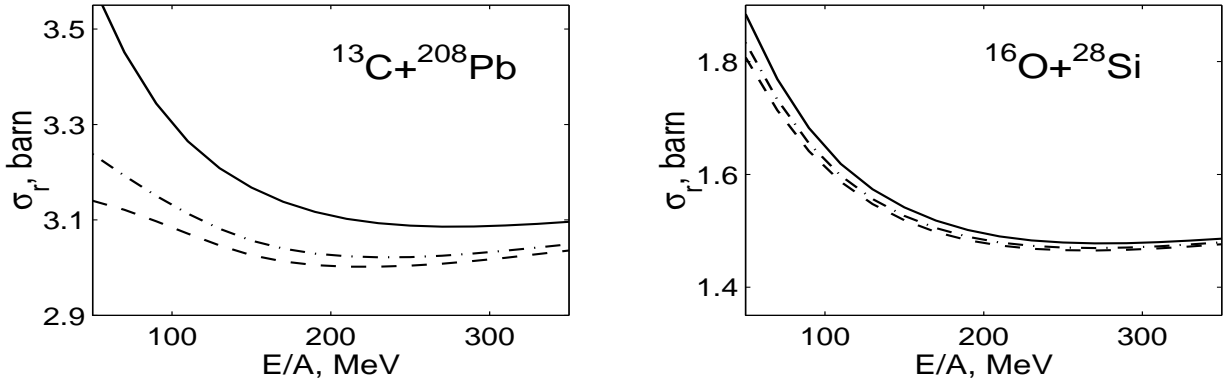


Figure 6: Trajectory distortion effects on cross-sections. Solid curves – no distortions; dashes – only the Coulomb distortion included; dashes-dots – effect of the Coulomb and nuclear distortion. For parameters see the text.

the turning point b_c in the Coulomb field

$$b \rightarrow b_c = \bar{a} + \sqrt{\bar{a}^2 + b^2}, \quad (4.4)$$

where $\bar{a} = Z_p Z_t e^2 / 2E_{c.m.}$ is the half-distance of the closest approach in the field $Z_p Z_t e^2 / r$ at $b = 0$. Later, the procedure of exchanging b by b_c was also used for the nuclear part of the phase $\Phi_N(b)$ in calculations of differential cross-sections of elastic scattering [13], and, in general, it proved to be correct (see, for instance, [39]). In addition, at peripheral collisions one can account for a contribution of the real part $V(r)$ of an attractive nuclear potential, which brings the Coulomb trajectory closer to the target-nucleus. If one assumes the region $b \geq R_s = R_p + R_t + (a_p + a_t) \ln 2$ to be the main for elastic scattering where the nuclear densities overlap less than $1/3$ of their values in the center [19], then the influence of the "tail" of the nuclear potential can be taken into account by exchanging

$$b \rightarrow \tilde{b}_c = \tilde{a} + \sqrt{\tilde{a}^2 + b^2}, \quad (4.5)$$

where $\tilde{a} = (Z_p Z_t e^2 - R_s |V(R_s)|) / 2E_{c.m.}$. A more refined way of inclusion of nuclear distortion was elaborated in [40] and applied in a series of works (see, for example, [14]). Nevertheless, if the optical potential itself is obtained by numerical fitting to experimental data, then the use of its real part to correct the Coulomb trajectory in calculations of the reaction cross-sections σ_R loses its meaning. Indeed, in these cases the data on σ_R are usually included into the fit procedure, or, if they are not available, then they themselves are calculated on the basis of the S_l -matrix elements obtained by fitting the differential cross-sections of elastic scattering only. Often these "calculated" σ_R data are called "experimental" cross-sections. So the use of the nuclear trajectory distortion is meaningful only for construction of eikonal phases of distorted waves when calculating direct inelastic and nucleon removal reactions. Another situation is when the real part of the nucleus-nucleus potential is calculated, for example, using the double-folding method. Then it is reasonable to calculate both the differential and total cross-sections in the Glauber-Sitenko approach taking into account the trajectory distortion by both the Coulomb and nuclear field.

Figure 6 demonstrates the calculations by (3.17) of the total cross-sections for $^{13}\text{C} + ^{208}\text{Pb}$ and $^{16}\text{O} + ^{28}\text{Si}$ without including trajectory distortion (solid curves), with the Coulomb distortion only, using the method (4.4) (dotted), and with the Coulomb and nuclear distortion by

the method (4.5) (dash-dotted). In the last case one should specify the parameters of the nucleus-nucleus potentials, and for $^{13}\text{C}+^{208}\text{Pb}$ we took them from [41] (the "C-potential" at 390 MeV), and for $^{16}\text{O}+^{28}\text{Si}$ from [42] (the "E-potential" at 215.2 MeV). In computing phases, we used for ^{13}C the parameters of the ^{12}C point-like density from Table 2. The parameters of ^{16}O are also given in Table 2. For ^{208}Pb and ^{28}Si , the parameters were computed with the help of (4.3) using the values R and a from Table 1. As expected, the inclusion of Coulomb distortion leads to appreciable corrections, of the order of 10100 MeV/nucleon and less, which is beyond experimental errors. As the collision energy increases, these corrections diminish and for lighter targets-nuclei (the right-hand part of Fig.6) they reach about 2they can be neglected. Contribution of the nuclear distortion is poor in comparison with the Coulomb one for ^{208}Pb and comparable with this for the reaction on the ^{28}Si -target, although in the latter case both the effects give small contributions. Besides, it is necessary to bear in mind that the real part of the nuclear potential decreases with increasing energy, but this was not taken into account.

4.4 In-medium effects

In the microscopic approach we deal with the total cross-section $\sigma_{NN}(\varepsilon_{lab})$ of the NN-scattering of free nucleons. This cross-section depends on energy, and thus defines the main dependence of the nucleus-nucleus cross-section on the collision energy $E_{lab} = \varepsilon_{lab} A_p$. We have taken the parametrization of $\sigma_{NN}(\varepsilon_{lab})$ from [23] in the energy interval $\varepsilon_{lab} = 10 \text{ MeV} \div 1 \text{ GeV}$. More generally, one should take into account the in-medium effect on the nucleon-nucleon interactions in nuclear matter. Usually, for this aim the cross-section is multiplied by the factor f_m , and therefore, in the convolution integral the isospin averaged cross-section (2.3) is exchanged as follows:

$$\sigma_{np} \Rightarrow \sigma_{np} \times f_m(np), \quad \sigma_{pp} = \sigma_{nn} \Rightarrow \sigma_{nn} \times f_m(nn). \quad (4.6)$$

The factors $f_m(np)$ and $f_m(nn)$ depend of the nucleon energy $\varepsilon_{lab} = E_{lab}/A$ and on the density of nuclear matter. The problem of the in-medium corrections of the NN-forces has been investigated in many works. So in [43], based on the Dirac-Bruckner approach for nuclear matter, numerical calculations were made of the total NN cross-sections. Parameterization of these calculations was given in [44] in analytic form for the correction factors

$$f_m(np) = \frac{1 + 20.88 \varepsilon_{lab}^{0.04} \rho^{2.02}}{1 + 35.86 \rho^{1.90}}, \quad f_m(nn) = \frac{1 + 7.772 \varepsilon_{lab}^{0.06} \rho^{1.48}}{1 + 18.01 \rho^{1.46}}. \quad (4.7)$$

Here the energy is given in MeV , and the density in fm^{-3} . One can see that for free nucleons when $\rho = 0$, we have $f_m(np) = f_m(nn) = 1$, and as the density increases these factors f_m vanish, as well as the corresponding effective cross-sections⁹. It is difficult to compute the convolution integrals with correction factors in the form (4.7) including the dependence on r , and we limit ourselves to qualitative estimations only. In Fig.7 are shown such calculations when the values of nuclear densities in (4.7) are assumed to be constants $\rho = \bar{\rho} = \bar{\rho}_p + \bar{\rho}_t$ for every region where the colliding nucleons can be. Then, denoting by $\rho_0 = \rho_p(0) + \rho_t(0)$ the net density in the centers of colliding nuclei, we show the calculated cross-sections when the f_m factor are taken

⁹ In the microscopic models of the double-folding potentials the same problems arise when constructing the energy and in-medium dependence of NN-potentials. However, the advantage of the Glauber-Sitenko approach is that the main dependence of energy is already included in parametrization of the total σ_{NN} cross-sections of free nucleons.

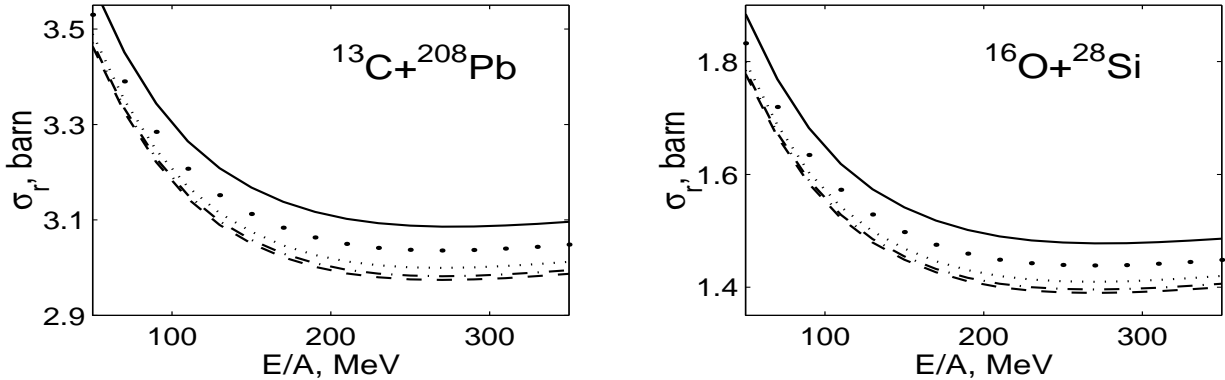


Figure 7: In-medium effect on cross-sections. Solid curves – no in-medium dependence ($\bar{\rho}=0$); bold dots are when the density in the overlap region is taken as $1/20\rho_0$ with $\rho_0 = \rho_p(0) + \rho_t(0)$ expressed through densities at the centers of nuclei; dots – for overlap with $1/6\rho_0$; dashes-dots – for $1/3\rho_0$; dashes – at ρ_0 .

for free nucleons (at $\bar{\rho}=0$, solid lines), and also for nucleons in the medium at $\bar{\rho}=(1/20)\rho_0$ (bold lines), $(1/6)\rho_0$ (dots), $(1/3)\rho_0$ (dash-dotted lines), ρ_0 (dashed curves). It is seen that the inclusion of the in-medium factors f_m can diminish the total reaction cross-section by 4-7% and that the dependence on the density turns out to be strongly nonlinear.

5 Conclusions, comparison with experimental data

1. It is shown that the initial expression for the microscopic eikonal phase can be represented in a convenient form where one of two density thickness functions of point-like nucleons in nuclei transforms into the profile of a nuclear density obtained from independent experimental data, e.g., from nuclear form factors. Ultimately, it turns out that in calculations of nucleus-nucleus cross-sections it is not necessary to introduce free parameters but, instead, to base on the known experimental data, only.

2. The main problem of the microscopic approach is to calculate eikonal scattering phases. For this aim, many people use the simplest nuclear densities in the form of Gaussian functions. Instead, here we demonstrate how one can use the realistic density distributions in the form of (symmetrized) Fermi functions, whose parameters are known for many nuclei. In this case, all functions in the eikonal integrals turn out to be given in the explicit form, which highly simplifies numerical calculations.

3. Two methods of obtaining the radius c and diffuseness d parameters of the point-like density $\rho_{SF}^0(r, c, d)$ are presented. One of them deals with nuclear form factors, and the other obtains these parameters from the known nuclear densities $\rho_{SF}(r, R, a)$. It turns out that the difference between the cross-sections calculated by using these two sets of parameters can achieve the value beyond the bars of typical experimental cross-sections. We conclude that a more justified method is that based on the analysis of form factors of nuclei obtained by subtracting the nucleon form factor and, if necessary, the form factor of the nuclear center-of-mass motion, as was carried out, for example, in [29].

4. In calculation, it was established that the *rms* radii of the nucleon-nucleon interaction $r_{N\,rms}^2$ and of the nucleon itself $r_{0\,rms}^2$ may be considered to be equal. The slight difference

between them is in the range of accuracy of their evaluation, and this does not affect practically the results of calculations of the nucleus-nucleus total reaction cross-sections. At the same time at $r_{N\,rms}^2 = r_{0\,rms}^2$ the convolution integrals take highly simple forms (2.16), (2.17) where only two profile functions overlap, one is for the nuclear density and the other is for the point-like density. Next, the convolution integral takes a simple one-dimensional form.

5. In many typical cases one should take into account a Coulomb trajectory distortion by means of the formal replacing, in the phase $\chi(b)$, the impact parameter b by b_c , according to (4.4). Additional distortion of the trajectory by the tail of a nuclear potential is not reasonable because its parameters are to be fitted, in particular, to the same data on total cross-sections.

6. The question whether the in-medium factor f_m for corrections of the NN-cross-sections should be taken into consideration remains open for us till now. The estimations show that at intermediate energies this factor does not change substantially the nucleus-nucleus total cross-sections. Nevertheless, the use of the above given factors $f_m(np)$ and $f_m(nn)$ from [44] hinder the usual calculations. Other authors faced similar obstacles, for example, when solving a simpler problem of the pA scattering data analysis [45]. Besides, in both these works, the Gaussian functions were chosen as the basic nuclear densities, while their replacing by the realistic ones can change the conclusions about the structure of the factors f_m as compared to those given by eq.(4.7). For example, successful agreement of calculations with the data on total reaction cross-sections for a series of reactions pA , αA and $^{12}C + ^{12}C$ was obtained in [46] with realistic densities and with the factors f_m differing in form from those given above ¹⁰.

7. Our calculations show that in the case of relatively light incident nuclei, it is more profitable to use the convolution integral (3.17) with the thickness function $\rho_p^\circ(s)$ for the point-like density of the projectile nucleus in the form of the modified Gaussian \bar{G} -function. The latter is determined with the help of (3.6) and (3.7) by means of parameters of realistic SF-function taken, for example, from Table 2. In the case of heavier incident nuclei it is advantageous to use the convolution integral (2.16) where one can insert the known explicit form of the Fourier-Bessel profiles of realistic SF-densities (3.22) for both the nuclei. In all calculations the Coulomb distortion of trajectory should be first of all taken into account.

8. We emphasize that in the existing literature no attention is focused on the problem of correct use of the initial formula for the convolution integral. From the above discussion it is evident that if the finite radius of the NN-interaction ($a_N^2 \neq 0$) is taken into account explicitly, both the densities must be taken as densities of nuclei for the point-like nucleons. Further, when the rms-radii of the nucleon and the NN-interaction are equal to each other, the NN-interaction factor disappears in the convolution integral, but one of the point-like densities is transformed to the nuclear one. However, in this case, the absence of the NN-factor $f(\xi)$ does not mean that one uses the zero-range approximation. The confusion arises also, when one assumes $a_N^2 = (2/3)r_{N\,rms}^2 = 0$ in (2.4) and calls this case the zero-range approximation, while at the same time takes for both the densities the table data, i.e., just the nuclear densities, instead of the point-like ones.

In Fig.8a,b, our calculations are compared with the experimental data collected in [49]. The SF-density parameters are given in Table 1. For the density ρ_{SF}° the parameters c and d of the projectile ^{12}C are given in Table 2, and for the incident nucleus ^{20}Ne they are calculated with the help of (4.3) and the data from Table 1. The convolution integral has been taken in the form of (3.17). Only the Coulomb trajectory distortion was taken into account. Thus,

¹⁰ In calculations of the real part of the double-folding nucleus-nucleus potential, the in-medium effect on the NN-potential is parametrized by simpler factors f_m in the form of the step and exponential functions of densities $\rho(r)$ (see., e.g., [47]).

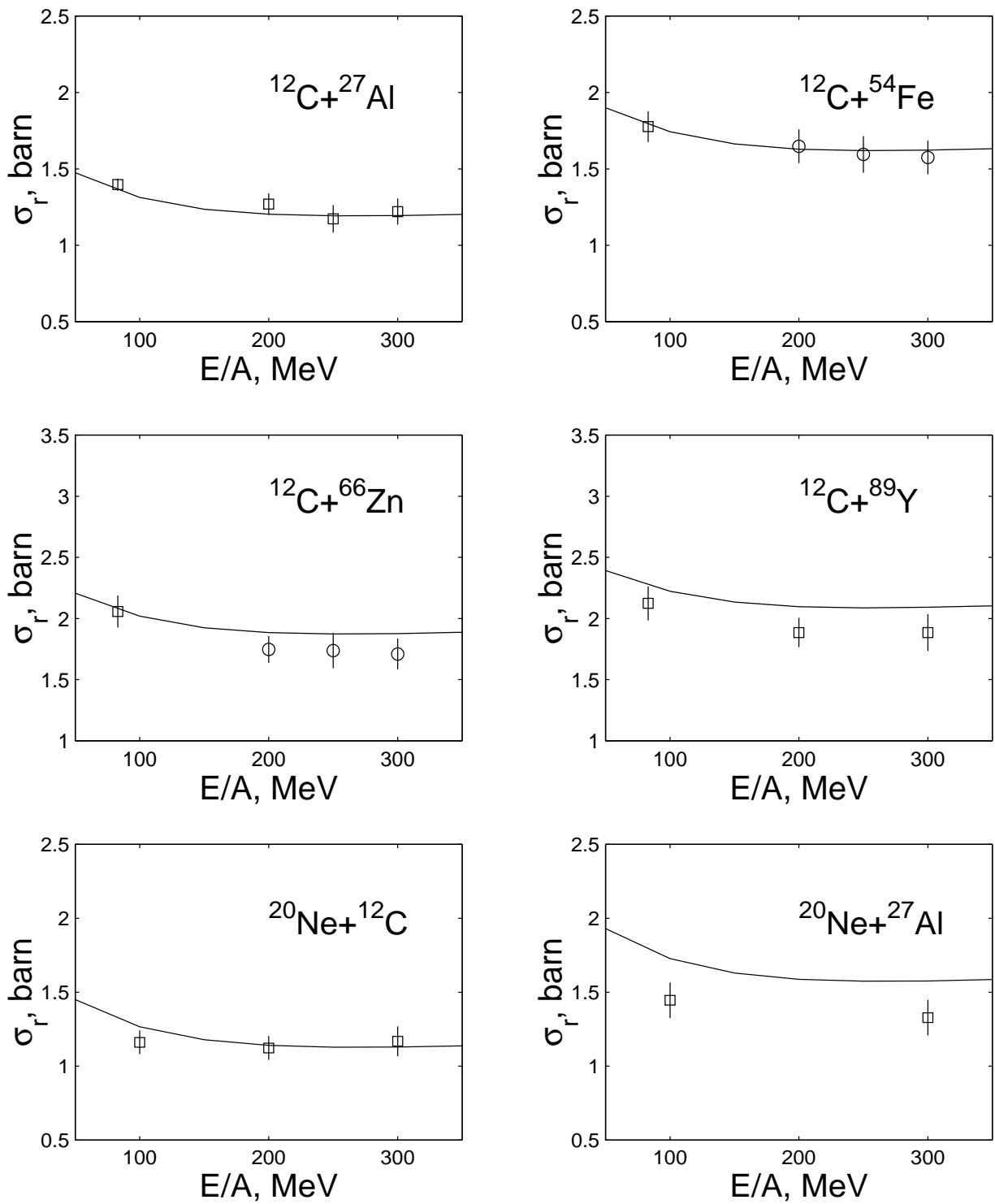


Figure 8: Calculated cross-sections compared with experimental data from [48]. Parameters are from the eA -scattering data (see in the text). Only the Coulomb distortion is included.

no free parameters have been introduced. One can see that in all cases a good agreement with experimental data is observed, except for $^{12}C + ^{89}Y$ and $^{20}Ne + ^{27}Al$. In the latter cases, some discrepancies can be due to the fact that the parameters for densities of the odd nuclei ^{89}Y and ^{27}Al were obtained from eA form factors (for references see [28]) with the help of formulae for spinless nuclei. However, if one introduces the in-medium factor f_m , the mentioned disagreements can be removed. Nevertheless, we believe that first of all one should improve the data on geometric parameters of the given nuclei. The other remark is that calculations of cross-sections in [48] with the help of Gaussian functions [22], which reproduce the behavior of "tails" of densities, give enhanced values which are beyond the experimental bars shown in Figs.8a,b. This is conceivable that in [48] they took the nuclear densities instead of the point-like ones, as it was mentioned above. On the other hand, calculations in [49] with the uniform density distributions for the target-nuclei and Gaussian functions for the projectiles give underestimations of the cross-sections for $^{20}Ne + ^{12}C$ and $^{12}C + ^{27}Al$, in spite of that they, probably, use not the point-like but nuclear densities for estimations of *rms*-radii needed to get the step radius R_u in (3.3). So, this result confirms that shown in Fig.3.

In conclusion, the authors would like to thank the Infeld-Bogolubov Foundation for its support, and E.B.Z. acknowledges the support of the Russian Foundation for Basic Research (grant 0001-006-17).

References

- [1] R.J.Glauber, *Lectures on Theor. Phys.*, **1** (Interscience, New York, 1959).
- [2] .G.Sitenko, Ukr.Fiz.J. **4** 152 (1959);
- [3] G.D.Satchler, *Direct nuclear reactions* (Clarendon, Oxford, 1983).
- [4] V.K.Lukyanov, B. Slowinski, E. Zemlyanaya, Yad.Fiz. **64** 1349 (2001);
V.K.Lukyanov, B. Slowinski, E. Zemlyanaya, Phys.At.Nucl.**64**
- [5] J.-S.Wan a.o., Kerntechnik **63** 167 (1998).
- [6] L.W.Townsend, J.W.Wilson, Rad.Res. **106** 283 (1986).
- [7] S.Fernbach, R.Serber, T.B.Taylor, Phys.Rev. **75** 1352 (1949).
- [8] W.Czyz, L.S.Maximon, Ann.of Phys. **52** 59 (1969).
- [9] J.Formanek, Nucl.Phys.B **12** 441 (1969).
- [10] I.Tanihata, J.Phys.G **22** 157 (1996).
- [11] C.A.Bertulani, L.F.Cano, M.S.Hussein, Phys.Rep. **226** 281 (1993).
- [12] O.M.Knyaz'kov, I.N.Kukhtina, S.A.Fayans, Fiz.Elem.Chast.& At.Yad.**28** 1061 (1997);
O.M.Knyaz'kov, I.N.Kukhtina, S.A.Fayans, Sov.J.Part.Nucl. **28** 418 (1997).
- [13] A.Vitturi, and F.Zardi, Phys.Rev.C **36** 1404 (1987).
- [14] Moon Hoe Cha, Phys.Rev.C **46** 1026 (1992).
- [15] C.E.Aguiar, F.Zardi, A.Vitturi, Phys.Rev.C **56** 1511 (1997).
- [16] J.A.Tostevin, R.C.Johnson, J.S.Al-Khalili, Nucl.Phys.A **630** 340c (1998).
- [17] G.F.Bertsch, B.A.Brown, H.Sagava, Phys.Rev.C **39** 1154 (1989).
- [18] G.D.Alkhazov, V.V.Anisovich, P.E.Volkovitskiy, *Diffractive interactions of hadrons with nuclei at high energies* (Nauka, Leningrad, 1991) (in russian).
- [19] G.R.Satchler and W.G.Love, Phys.Rep. **55** 183 (1979).
- [20] O.D.Dalkarov, V.A.Karmanov, Nucl.Phys.A **445** 579 (1985).
- [21] H.M.Fayyad, T.H.Rihan, A.M.Awin, Phys.Rev.C **53** 2334 (1996).
- [22] P.J.Karol, Phys.Rev.C **11** 1203 (1975).
- [23] S.Charagi and G.Gupta, Phys.Rev.C **41** 1610 (1990).

- [24] Yu.N.Eldyshev, V.K.Lukyanov, Yu.S.Pol', *Yad.Fiz.* **16** 506 (1972);
Yu.N.Eldyshev, V.K.Lukyanov, Yu.S.Pol', *Sov.J.Nucl.Phys.* **16** 282 (1973).
- [25] D.W.L.Sprung, J.Martorell, *J.Phys.A* **30** 6525 (1997); *ibid.* **31** 8973 (1998).
- [26] M.Grypeos, C.Koutroulos, V.Lukyanov, A.Shebeko, *J.Phys.G* **24** (1998) 1998.
- [27] V.V.Burov, D.N.Kadrev, V.K.Lukyanov, Yu.S.Pol', *Yad.Fiz.* **61** 595 (1998);
V.V.Burov, D.N.Kadrev, V.K.Lukyanov, Yu.S.Pol', *Phys.At.Nucl.* **61** 525 (1998).
- [28] De Vries H., de Jager C.W., de Vries C., *At. Data & Nucl. Data Tables* **36** (1987) 495.
- [29] V.V.Burov, V.K.Lukyanov, *Preprint P4-11098, JINR (Dubna, 1977).*
- [30] V.K.Lukyanov, E.V. Zemlyanaya, *J.Phys.G.* **26** 357 (2000).
- [31] I.Gradshteyn, I.Ryzhik, *Tables of Series, Products and Integrals* (H.Deutsh, 1987)(Engl.transl.).
- [32] M.Abramowitz and I.A.Stegun, *Handbook of Mathematical Functions*, (Nat. Bureau of Standards, Appl. Math. Series, 1964).
- [33] M.E.Grypeos, C.G.Koutroulos, V.K.Lukyanov, A.V.Shebeko, *Fiz.Elem.Chast.& At.Yad.* **32** 1494 (2001);
M.E.Grypeos, C.G.Koutroulos, V.K.Lukyanov, A.V.Shebeko, *Phys.Particles&Nucl.*, **32** 779 (2001).
- [34] I.Zh. Petkov, V.K.Lukyanov, Yu.S.Pol', *Yad.Fiz.*, **4** 57 (1966).
- [35] I.Zh. Petkov, V.K.Lukyanov, Yu.S.Pol', *Yad.Fiz.*, **9** 349 (1969).
- [36] S.Fälldt, A. Ingemarsson, *J.Phys.G.* **9** 261 (1983).
- [37] M.El-Azab Farid, G.R.Sachler, *Nucl.Phys.A* **438** 525 (1985).
- [38] R.M.DeVries, and J.C.Peng, *Phys.Rev.* **22** 1055 (1980).
- [39] V.K.Lukyanov, E.V. Zemlyanaya, *Int.J.Mod.Phys.E.* **10** no.3, 169 (2001).
- [40] D.M. Brink, and G.R.Satchler, *J.Phys.G.* **7** 43 (1981).
- [41] M.Buenerd et al., *Nucl.Phys.A* **bf 424** 313 (1984).
- [42] G.R.Sachler, *Nucl.Phys.A* **bf 279** 493 (1977).
- [43] G.Q.Li and R Machleidt, *Phys.Rev.* **48** 1702 (1993); *ibid.* **49** 566 (1994).
- [44] Cai Xiangzhou, Feng Jun, Shen Wenqing, Ma Yugang, Wang Jiansong, and Ye Wei, *Phys.Rev.* **58** 572 (1998).
- [45] A.de Vismes, P.Roussel-Chomaz, and R.Carstoiu, *Phys.Rev.* **62** 064612-1 (2000).
- [46] R.K.Tripathi, J.W.Wilson, F.A.Cucinotta, *Nucl.Instr.& Meth.Phys.Res.B* **145** 277 (1998).
- [47] Dao T.Khoa, G.R.Satchler, W.von Oertzen, *Phys.Rev.C* **56** 954 (1997).
- [48] S.Kox et al, *Phys.Rev.C* **35** 1678 (1987).
- [49] A.Y.Abul-Magd, M.Talib Ali-Alhinai, *Nuovo Cim.A* **110** 1281 (1997).